Multipolar magnetism in *d*-orbital systems: Crystal field levels, octupolar order, and orbital loop currents

Sreekar Voleti [1] D. D. Maharaj [2] B. D. Gaulin,[2,3,4] Graeme Luke,[2,3,5] and A. Paramekanti[1,*]

[1]*Department of Physics, University of Toronto, 60 St. George Street, Toronto, Ontario, Canada M5S 1A7*
[2]*Department of Physics and Astronomy, McMaster University, Hamilton, Ontario, Canada L8S 4M1*
[3]*Brockhouse Institute for Materials Research, McMaster University, Hamilton, Ontario, Canada L8S 4M1*
[4]*Canadian Institute for Advanced Research, 661 University Ave., Toronto, Ontario, Canada M5G 1M1*
[5]*TRIUMF, 4004 Wesbrook Mall, Vancouver, British Columbia, Canada V6T 2A3*

Quantum magnets with spin $J = 2$, which arise in spin-orbit coupled Mott insulators, can potentially display multipolar orders. Motivated by gaining a better microscopic understanding of the local physics of such *d*-orbital quantum magnets, we carry out an exact diagonalization study of a simple octahedral crystal field Hamiltonian for two electrons, incorporating spin-orbit coupling (SOC) and interactions. While the rotationally invariant Kanamori interaction in the t_{2g} sector leads to a fivefold degenerate $J = 2$ manifold, we find that either explicitly including the e_g orbitals, or going beyond the rotationally invariant Coulomb interaction within the t_{2g} sector, causes a degeneracy breaking of the $J = 2$ levels. This can lead to a low-lying non-Kramers doublet carrying quadrupolar and octupolar moments and an excited triplet which supports magnetic dipole moments, bolstering our previous phenomenological proposal for the stabilization of ferro-octupolar order in heavy transition metal oxides. We show that the spontaneous time-reversal symmetry breaking due to ferro-octupolar ordering within the non-Kramers doublet leads to electronic orbital loop currents. The resulting internal magnetic fields can potentially explain the small fields inferred from muon-spin relaxation (μSR) experiments on cubic $5d^2$ osmate double perovskites Ba_2ZnOsO_6, Ba_2CaOsO_6, and Ba_2MgOsO_6, which were previously attributed to weak dipolar magnetism. We make further predictions for oxygen NMR experiments on these materials. We also study the reversed level scheme, where the $J = 2$ multiplet splits into a low-lying magnetic triplet and excited non-Kramers doublet, presenting single-ion results for the magnetic susceptibility in this case, and pointing out its possible relevance for the rhenate Ba_2YReO_6. Our work highlights the intimate connection between the physics of heavy transition metal oxides and that of *f*-electron based heavy fermion compounds.

Multipolar orders have been proposed and discussed extensively in *f*-orbital based heavy fermion compounds [1–14]. Such multipolar orders have also been proposed to occur in *d*-orbital metals with large spin-orbit coupling (SOC), such as $LiOsO_3$ and $Cd_2Re_2O_7$, via Pomeranchuk instabilities of the Fermi liquid [15]. Optical second-harmonic generation experiments on $Cd_2Re_2O_7$ have found evidence for such an inversion broken quadrupolar ordered state below $T_c \sim 200$ K [16]. Other candidates for multipolar orders include proposed quadrupolar order in A_2OsO_4 (with A = K, Rb, Cs) [17].

In recent work we have studied *d*-orbital Mott insulators with large SOC and a d^2 configuration in a local octahedral environment, and proposed these systems as candidates for realizing ferro-octupolar order [18,19]. Previous studies of such d^2 quantum magnets [20–22] have argued that the combination of crystal field and interaction effects leads to the stabilization of a state with total $L = 1$ and $S = 1$, which are locked by SOC into a $J = 2$ spin. Motivated by experiments

[18,23–26] on certain cubic double perovskite (DP) Mott insulators, Ba_2ZnOsO_6, Ba_2CaOsO_6, and Ba_2MgOsO_6, which host a $5d^2$ configuration on Os, we have instead proposed [19] that their observed nontrivial phenomenology, such as entropy and a spin gap, could be captured by assuming that the fivefold $J = 2$ multiplet is weakly split, resulting in a ground state non-Kramers doublet carrying quadrupolar and octupolar moments. The lack of any observed crystal distortions in x-ray and neutron diffraction experiments appears to rule out quadrupolar order [18]. Uniform ferro-octupolar ordering in the low lying doublet manifold then provides the most viable route to further reconciling the cubic symmetry, the observation of time-reversal symmetry breaking seen via μSR oscillations [23], the apparent lack of any magnetic Bragg peaks in elastic neutron diffraction experiments [18], and the spin gap observed in inelastic neutron scattering experiments [18,19].

In this paper we provide further theoretical calculations in favor of the above scenario. We first present exact diagonalization results on a simple local crystal field Hamiltonian keeping the t_{2g} and e_g levels in an octahedral environment, showing that the combination of SOC and interactions does

*arunp@physics.utoronto.ca

favor a non-Kramers ground state doublet. We show how the splitting between this doublet and the excited magnetic triplet depends on SOC and the Hund's coupling and results from perturbative t_{2g}-e_g mixing. Such t_{2g}-e_g mixing was discussed previously but its importance for the low energy physics appears not to have been properly recognized [21,27]. We also examine a model of just t_{2g} electronic states, and show that deviations of the Coulomb interaction from spherical symmetry, perhaps engendered by hybridization with oxygen orbitals [28], can lead to a similar non-Kramers doublet state. This doublet-triplet splitting may be too small to be resolved using resonant inelastic x-ray scattering experiments [29,30], but it is crucial for the low energy symmetry-breaking orders. We study the impact of ferro-octupolar order within this low energy non-Kramers doublet, and show that this leads to orbital electronic currents, generating internal magnetic fields and semiquantitatively explain the μSR oscillations seen in Ba$_2$ZnOsO$_6$, Ba$_2$CaOsO$_6$, and Ba$_2$MgOsO$_6$. The nonspherical Coulomb interaction mechanism for splitting the $J = 2$ multiplet discussed above also permits for the possibility for the level ordering to be reversed, with a magnetic triplet ground state and an excited non-Kramers doublet. We present single ion results for the magnetic susceptibility in this case, arguing that this reversed level scheme is likely to be relevant to the $5d^2$ rhenate [31] Ba$_2$YReO$_6$.

Our theory strengthens the case for multipolar orders in a class of d-orbital Mott insulators, pointing to a smooth conceptual link between the physics of heavy d-orbital oxides and f-electron based heavy fermion materials. Such octupolar order with a high transition temperature may provide a new template to store information.

I. LOCAL MODEL

We use the following Hamiltonian for two electrons in a d-orbital placed in an octahedral environment:

$$H = H_{\text{CEF}} + H_{\text{SOC}} + H_{\text{int}}, \quad (1)$$

where we include the octahedral crystal field splitting, SOC, and Kanamori interactions, written in the orbital basis ($\{yz, xz, xy\}, \{x^2 - y^2, 3z^2 - r^2\}$) $\leftrightarrow$ ($\{1, 2, 3\}, \{4, 5\}$) where $\alpha \equiv \{1, 2, 3\}$ label t_{2g} orbitals and $\alpha \equiv \{4, 5\}$ label e_g orbitals. The CEF term is given by

$$H_{\text{CEF}} = V_C \sum_{\alpha=4,5} \sum_s n_{\alpha,s}, \quad (2)$$

where s is the spin. The SOC term is

$$H_{\text{SOC}} = \frac{\lambda}{2} \sum_{\alpha,\beta} \sum_{s,s'} \langle \alpha | \mathbf{L} | \beta \rangle \cdot \langle s | \boldsymbol{\sigma} | s' \rangle c_{\alpha,s}^\dagger c_{\beta,s'}, \quad (3)$$

where $\boldsymbol{\sigma}$ refers to the vector of Pauli matrices, and $\mathbf{L}$ is the orbital angular momentum. Its components in the orbital basis are given in Appendix A. We assume a Kanamori interaction for all five d orbitals given by

$$H_{\text{int}} = U \sum_\alpha n_{\alpha\uparrow} n_{\alpha\downarrow} + U' \sum_{\alpha>\beta} n_\alpha n_\beta - J_H \sum_{\alpha\neq\beta} \vec{S}_\alpha \cdot \vec{S}_\beta$$
$$+ J_H \sum_{\alpha\neq\beta} c_{\alpha\uparrow}^\dagger c_{\alpha\downarrow}^\dagger c_{\beta\downarrow} c_{\beta\uparrow}, \quad (4)$$
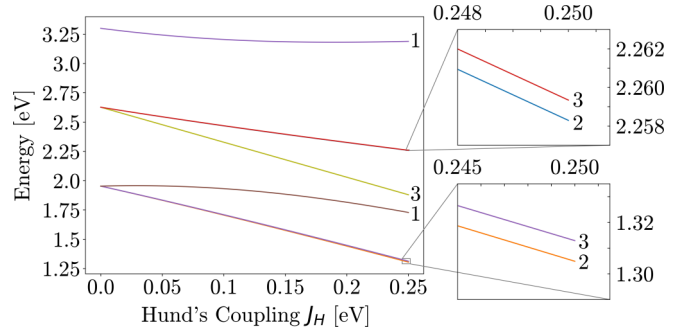

FIG. 1. Low energy spectrum (15 lowest eigenvalues) of the Hamiltonian in Eq. (1) with two electrons, corresponding to states where both electrons predominantly occupy the t_{2g} orbitals. The numbers at the end of the curves, and in the zoomed-in insets which show weak splittings, indicate the degeneracies of the different energy levels.

where $\vec{S}_\alpha = (1/2)c_{\alpha s}^\dagger \vec{\sigma}_{s,s'} c_{\alpha s'}$. This simple form, where we use the same interaction parameters for all t_{2g} and e_g orbitals, is used to avoid a proliferation of interaction parameters. Assuming spherical symmetry of the Coulomb interaction, we have $U' = U - 2J_H$ (see, e.g., Ref. [32]).

For electronic configurations with partially filled t_{2g} orbitals, the most commonly used approach is to simply ignore the e_g orbitals and restrict attention to the low energy t_{2g} states. We find that the ground state manifold in this approximation consists of a fivefold degenerate $J = 2$ state. However, we show below that this degeneracy is further split due to two possible microscopic mechanisms: t_{2g}-e_g mixing and deviations of the Coulomb interaction from spherical symmetry.

A. t_{2g}-e_g mixing: Exact results, perturbation theory

We consider two electrons in the full d-orbital manifold including t_{2g} and e_g states, and study this using numerical exact diagonalization in the 45 basis states. For coupling constants we use values typical for $5d$ transition metal oxides: $V_C = 3$ eV, $U = 2.5$ eV, $\lambda = 0.4$ eV, and $J_H = 0.25$ eV. Figure 1 plots the evolution with J_H of the lowest 15 energy levels which correspond to eigenstates where the two electrons are predominantly both in the t_{2g} sector. The indicated numbers mark the degeneracies of these multiplets. For $J_H = 0$, there are just three energy levels, which, in increasing order of energy, correspond to having (i) both electrons in $j = 1/2$, (ii) one electron in $j = 1/2$ and one electron in $j = 3/2$ (energy cost $3\lambda/2$), and (iii) both electrons in $j = 3/2$ (energy cost 3λ). We see that the lowest energy set of five states evolves adiabatically out of the first sector as we increase J_H; this set of five states corresponds to the $J = 2$ moment. However, a zoom-in of this multiplet, as well as of one of the higher energy multiplets, shows that the apparent fivefold degeneracy of these states is actually weakly broken as $2 \oplus 3$ due to weak t_{2g}-e_g mixing. In particular, the naively expected fivefold degenerate $J = 2$ ground state is split into a non-Kramers doublet ground state and an excited magnetic triplet; for the typical values listed above, this splitting is $\sim$8 meV.

Figure 2 shows the dependence of this lowest energy doublet-triplet energy splitting (blue solid line) on V_C. We find
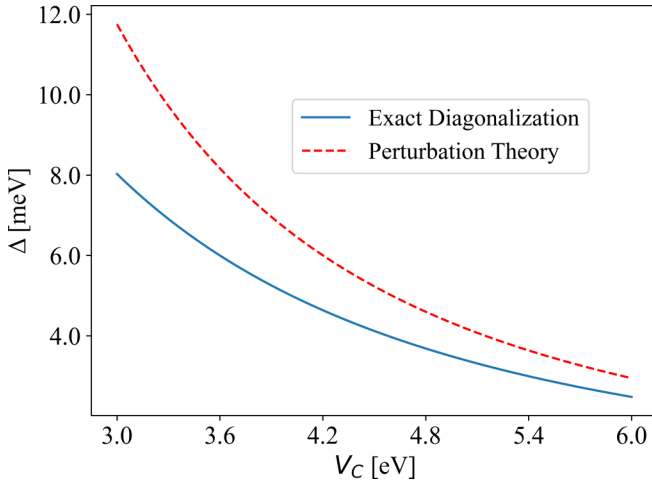
FIG. 2. Energy difference between the lower energy non-Kramers doublet (E_d) and the excited triplet (E_t), given by $\Delta = E_t - E_d$, obtained via exact diagonalization of the Hamiltonian in Eq. (1) (blue, solid line) plotted as a function of the dominant t_{2g}-e_g splitting V_C. We compare this with the third-order perturbation theory result (red, dashed line) induced by small ($J_H/V_C, \lambda/V_C$) which leads to weak t_{2g}-e_g mixing.

FIG. 3. Energy difference $\Delta = E_t - E_d$ between the magnetic triplet and the non-Kramers doublet obtained via exact diagonalization of the t_{2g}-only model, shown as a function of the normalized deviation $\delta U'/U'$ of the Coulomb interaction from spherical symmetry. For $\delta U' > 0$, the non-Kramers doublet has lower energy so $\Delta > 0$.

that this splitting can be semiquantitatively captured within third-order perturbation theory, as discussed in Appendix B, where we first eliminate the e_g states, to find an effective t_{2g} model, and then diagonalize this reduced Hamiltonian. The relevant terms arise at $O(\lambda^2 J_H/V_C^2)$, from the following sequence: (i) SOC λ promoting one electron from the t_{2g} manifold into the e_g sector, (ii) intermediate state t_{2g}-e_g interactions driven by Hund's coupling set by J_H, and finally (iii) de-exciting back via SOC λ to end up with both electrons in the t_{2g} manifold. Diagonalizing this third-order perturbative Hamiltonian, in conjunction with the bare t_{2g} Hund's coupling, leads to the non-negligible splitting shown (red dashed line) in Fig. 2, which agrees well with the full numerical calculation in the regime of large V_C. Our result is in contrast with a previous conjecture that the splitting would appear at fourth order in perturbation theory [21], which would have indeed rendered this effect negligible. This highlights a nontrivial effect of t_{2g}-e_g mixing, showing that it can be important for nucleating multipolar order in 5*d* Mott insulators. However, this effect by itself may be too small to account for the spin gap observed in neutron scattering experiments [18,19] on Ba_2ZnOsO_6, Ba_2CaOsO_6, and Ba_2MgOsO_6. We next turn to an additional mechanism, which can cooperate to enhance this splitting, or even reverse the level ordering which we argue is important in certain other materials.

B. Nonspherical Coulomb interactions in t_{2g} model

The second important physical effect we consider is that projecting the Coulomb interaction to the t_{2g} Wannier orbitals can lead to deviations from the spherical symmetry assumption, so that $U' \neq U - 2J_H$. This is expected to be more important for 5*d* orbitals which have more significant overlap with the oxygen cage, as has been previously noted in an *ab initio* study [28]. We therefore numerically diagonalize
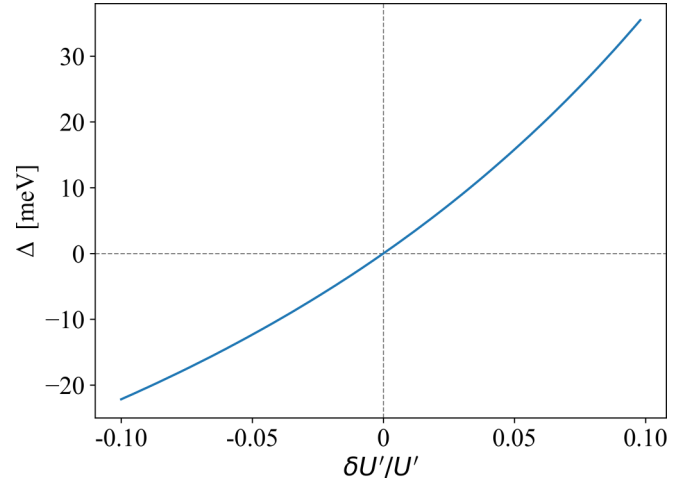
the above model Hamiltonian, restricting ourselves to the Hilbert space where both electrons occupy the t_{2g} orbitals, and varying $\delta U' = U' - (U - 2J_H)$ to simulate the deviation from spherical symmetry. Figure 3 shows how the low energy degeneracy gets split as we go away from $\delta U' = 0$. We see from here that even a small deviation $\delta U'/U' \sim 0.1$ leads to a substantial splitting ~ 20 meV. For $\delta U' > 0$, we find that the non-Kramers doublet is lower in energy than the magnetic triplet, which we argue is relevant to osmates such as Ba_2ZnOsO_6, Ba_2CaOsO_6, and Ba_2MgOsO_6. The case where the $\delta U' < 0$, so that the magnetic triplet lies lower in energy than the doublet, may be important to understand aspects of the unusual magnetism of the rhenate [31] Ba_2YReO_6; this will be discussed in Sec. III.

II. MAGNETIC FIELDS FROM OCTUPOLAR ORDER

On phenomenological grounds, and the above microscopic calculations, 5d^2 oxides are candidates for a low-lying non-Kramers doublet. As shown previously [19], this doublet may be described using the wave functions of the $J = 2$ manifold in terms of $|J_z\rangle$ eigenstates written as pseudospin-1/2 states:

$$|\psi_{g,\uparrow}\rangle = |0\rangle; \quad |\psi_{g,\downarrow}\rangle = \frac{1}{\sqrt{2}}(|2\rangle + |-2\rangle). \quad (5)$$

Each of these two states is individually time-reversal invariant. The angular momentum operators $(J_x^2 - J_y^2)$ and $(3J_z^2 - J^2)$, restricted to this basis, act as pseudospin-1/2 operators (τ^x, τ^z), forming the two components of an XY-like quadrupolar order parameter, while $\overline{J_xJ_yJ_z}$ (with overline denoting symmetrization) behaves as τ^y, and serves as the Ising-like octupolar order parameter. The mean field ferro-octupolar ordered ground state is described by each site being in the superposition state $|\psi_\pm^{\text{oct}}\rangle = |\psi_{g,\uparrow}\rangle \pm i|\psi_{g,\downarrow}\rangle$. Here the signs reflect the Z_2 nature of the Ising order, and i reflects the breaking of time-reversal symmetry.

The broken time-reversal symmetry of the octupolar ground state would lead to internal magnetic fields in the crystal. Using exact diagonalization, we obtain $|\psi_\pm^{\text{oct}}\rangle$ as the two-electron wave function obtained by superposing the two degenerate time-reversal invariant ground eigenstates as above, and compute the electronic currents in these states which generate the internal magnetic fields. In the single-site picture, the orbital currents responsible for the internal fields live on the d^2 ion. We thus define the orbital current density operator as

$$\mathbf{J}(\mathbf{r}) = \frac{ie\hbar}{2m} \sum_s [\Psi_s^\dagger(\nabla\Psi_s) - (\nabla\Psi_s^\dagger)\Psi_s], \qquad (6)$$

where s sums over the physical electron spin. We expand the operator Ψ in the orbital basis as

$$\Psi_s^\dagger = \sum_\alpha \psi_{n\ell\alpha}(r,\theta,\phi)c_{\alpha,s}^\dagger, \qquad (7)$$

where $\mathbf{r} \equiv (r,\theta,\phi)$, $\psi_{n\ell\alpha}$ refers to the real hydrogenlike wave function, with $n=5$ and $\ell=2$ for the $5d$ wave functions, and α denotes the orbital. We thus arrive at the spatially varying expectation value of the current density operator:

$$\langle\mathbf{J}(\mathbf{r})\rangle_\pm = \frac{ie\hbar}{2m} \sum_s \sum_{\alpha\beta} \langle\psi_\pm^{\text{oct}}|c_{\alpha,s}^\dagger c_{\beta,s}|\psi_\pm^{\text{oct}}\rangle\, \boldsymbol{\xi}_{\alpha\beta}, \qquad (8)$$

$$\boldsymbol{\xi}_{\alpha\beta} = R_{n\ell}^2(r)\big(Y_{\ell\alpha}\nabla Y_{\ell\beta} - Y_{\ell\beta}\nabla Y_{\ell\alpha}\big), \qquad (9)$$

where the two Ising states have $\langle\mathbf{J}(\mathbf{r})\rangle_- = -\langle\mathbf{J}(\mathbf{r})\rangle_+$. Here $Y_{\ell\alpha}(\theta,\phi)$ are real Tesseral harmonics, and $R_{n\ell}(r)$ is the radial wave function. To compute the current density, we use a variational ansatz for the radial wave function, which takes on a hydrogenic form, but with an effective nuclear charge which decreases with r, from a bare nuclear charge Z_0 for $r \to 0$ to the screened effective charge Z_∞ for $r \to \infty$, over a length scale r_0. For the Os^{6+} ion relevant to Ba_2ZnOsO_6, Ba_2CaOsO_6, and Ba_2MgOsO_6, we use $Z_0 = 76$ and $Z_\infty = 7$, and consider different values of r_0; details are given in Appendix B.

Using this expectation value for the current density, we compute the magnetic field via

$$\mathbf{B}_\pm(\mathbf{r}) = \frac{\mu_0}{4\pi} \int d^3r' \frac{\langle\mathbf{J}(\mathbf{r}')\rangle_\pm \times (\mathbf{r}-\mathbf{r}')}{|\mathbf{r}-\mathbf{r}'|^3}, \qquad (10)$$

where the integral is carried out over primed variables. The two Ising time-reversed partner states have opposite magnetic fields $\mathbf{B}_-(\mathbf{r}) = -\mathbf{B}_+(\mathbf{r})$.

The orbital current pattern which creates this field is shown schematically in Fig. 4 (left panel), highlighting that it is analogous to loop current orders proposed in certain cuprate and heavy fermion materials [33,34]. In a more realistic calculation, which retains hybridization with oxygen, the octupolar order we have uncovered may in fact be identical to plaquette loop current order in the OsO_6 cage. We find that the magnetic field has a pattern which, appropriately, might be expected from a set of eight alternating "magnetic monopoles" arranged on a cube, as shown in Fig. 4 (right panel), to form an octupole centered on the Os^{6+} ion. Figure 5 shows the magnetic field expected from these orbital currents as a function of distance from the Os^{6+} ion along the [111] direction, where the field
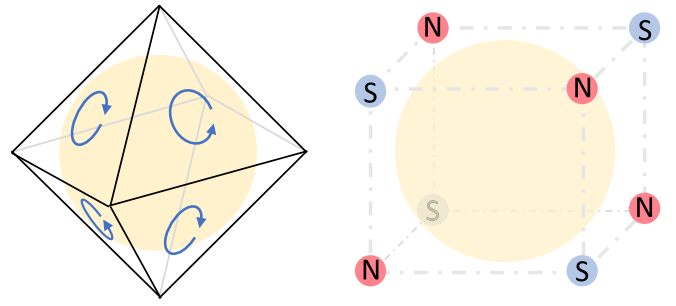

FIG. 4. Left: Schematic plot of the orbital current pattern on the $5d^2$ Os ion (indicated by the ball), showing that it has the same symmetry as plaquette loop current order residing on the OsO_6 octahedral cage. Right: Configuration of fictitious "magnetic monopoles" forming an octupole, which would produce the octupolar current loop pattern shown in the left panel.

strength is the largest, for two different choices of r_0 as indicated. Figure 6 shows the same calculation, but normalizing the field by that generated by a 1 μ_B dipole located at the Os^{6+} site.

While we have discussed above the magnetic field due to octupolar order as a function of distance from Os, in order to make a comparison with μSR experiments, we have to estimate the fields produced by the octupolar order at possible muon stopping sites. We thus next estimate the magnetic field distribution over the surface of a sphere of radius 1 Å centered around the oxygen site, which is where the muon is expected to be bound [35,36]. Figure 7 shows a plot of the field distribution, where we find the maximum field to be present at points on this sphere located near the Os^{6+} ion. (This calculation retained nine Os^{6+} ions closest to the oxygen ion, beyond which the contribution was negligible.) We note that these maxima lie between the $\langle 111 \rangle$ and $\langle 100 \rangle$ directions. The presence of four symmetric maxima of the
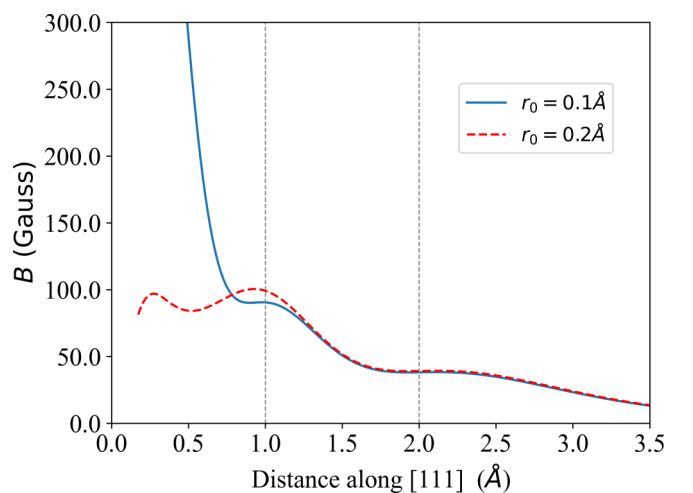

FIG. 5. Magnetic field generated within the crystal in the presence of ferro-octupolar order, plotted as a function of distance from the $5d^2$ Os ion along the [111] direction. The two curves correspond to different choices of the screening parameter r_0, which impacts the field only at short distances. The wiggles reflect the structure of the radial wave function.
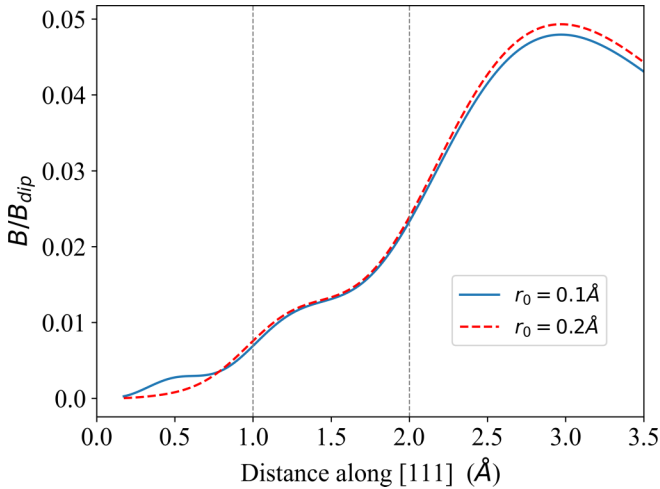
FIG. 6. Magnetic field in the presence of ferro-octupolar order, plotted as a function of distance from the $5d^2$ Os ion along the [111] direction. The data are the same as in Fig. 5, but normalized by B_{dip} which denotes the magnetic field at the same location generated by a 1 μ_B dipole moment located at the origin and pointing along the [111] direction.

field strength is consistent with the residual symmetry in the ferro-octupolar state of C_4 rotations about the Os-O axis followed by time reversal. The computed maximum field is found to be $\sim$30 G, within a factor of 2 of the $\sim$50 G magnetic field inferred from μSR experiments on Ba_2ZnOsO_6, Ba_2CaOsO_6, and Ba_2MgOsO_6 below a transition temperature T^*. A quantitative computation with the μSR results would need to retain the Os-O hybridization and *ab initio* calculations for the optimal muon stopping sites [35,36]. The magnetic field inferred from μSR experiments was previously attributed to possible weak magnetic dipolar order, with a tiny ordered moment $\lesssim 0.02$ μ_B. Such a tiny ordered moment is difficult to explain given the typical $\sim$1 μ_B local moments
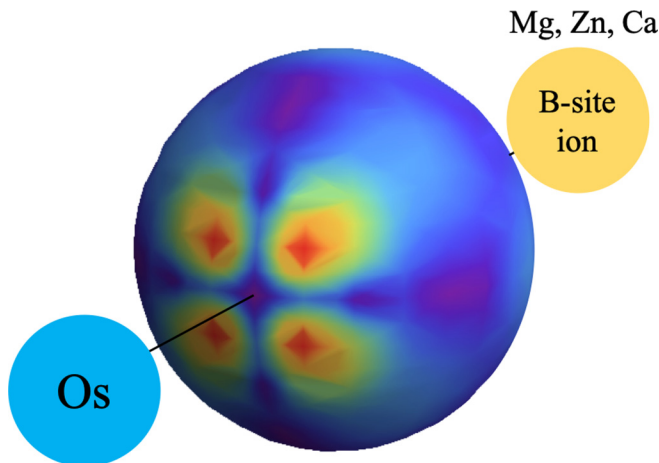

FIG. 7. Color plot of the ferro-octupolar magnetic field distribution over a sphere of radius 1 Å around the oxygen site where the muon is expected to be bound. The oxygen site is located half-way between Os and the B-site ion (Mg, Zn, Ca). The largest field strength (in red) appears near the Os^{6+} ion.
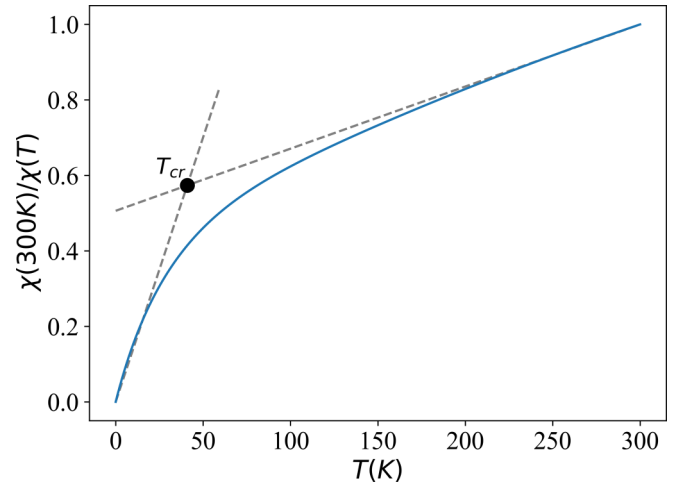

FIG. 8. Temperature dependence of the inverse magnetic susceptibility (normalized to its value at $T = 300$ K) in the single-site problem with a low lying magnetic triplet and an excited non-Kramers doublet; see text for details of the model and parameters. At high temperature, we find a Curie-Weiss-like linear form $\chi^{-1}(T) \propto (T + T_s)$, as indicated by the dashed line, with $T_s \sim 275$ K for the chosen parameters. At low temperature, we find the Curie law $\chi^{-1}(T) \propto T$. The temperature where the low T and high T lines meet denotes a crossover temperature scale $T_{\text{cr}} \approx 30$ K. Varying the doublet-triplet splitting, we find that $k_B T_{\text{cr}} \approx 0.07|\Delta|$ and $k_B T_s \approx 0.35|\Delta|$.

expected in such Mott insulators, unless one is fine tuned to be near a quantum critical point. Our work instead naturally rules out dipolar order, and instead explains this weak field as arising from loop currents in a phase which supports octupolar order.

III. REVERSED LEVEL SCHEME: MAGNETIC TRIPLET GROUND STATE

In previous work and in the above sections, we have extensively explored the case where the $J = 2$ multiplet is split into a low-energy non-Kramers doublet and a spin-gapped magnetic triplet. In this section we explore the single-ion physics of the reversed level scheme which has also not been studied in the oxides literature. As an illustrative example of a model which leads to this level ordering, we explore the Hamiltonian in Eq. (1), but with $\delta U' = U' - (U - 2J_H) < 0$, and projecting onto just the t_{2g} orbitals. We note that this deviation is not necessarily the only way in which the Coulomb interaction can deviate from spherical symmetry—indeed, imposing only the octahedral point group symmetry will allow for a broader set of interactions.

Figure 8 shows the inverse magnetic susceptibility $\chi^{-1}(T)$ in this single-ion case, normalized by its value at $T = 300$ K, for a choice of parameters $V_C = 3$ eV, $U = 2.5$ eV, $\lambda = 0.4$ eV, and $J_H = 0.25$ eV (as used in the previous sections), but with $\delta U' = -0.5$ eV. (This choice of an admittedly large $\delta U'$ is only used for the simplest model to illustrate the impact of splitting the lowest energy $J = 2$ multiplet; it is not meant to capture the full spectrum of higher energy excitations.) This leads to a triplet ground state, with an excited non-Kramers doublet at an energy $|\Delta| \sim 37$ meV. Interestingly, we find

that $\chi^{-1}(T) \propto (T + T_s)$ in this case, exhibiting an apparent "Curie-Weiss"-like form with $T_s \approx 275$ K, over a wide range of temperatures $\gtrsim 150$ K. Based on this, one might misleadingly infer a Curie-Weiss temperature ~ -275 K. Only upon going to lower temperatures, do we observe a change of slope and the correct $\chi^{-1}(T) \propto T$ Curie law associated with the single-ion low energy magnetic triplet. We find a very similar result in an even simpler model where we split the $J = 2$ multiplet using symmetry-allowed Stevens operators, via $H_{\text{eff}} = -V_{\text{eff}}(O_{40} + 5O_{44})$, with $V_{\text{eff}} < 0$, where

$$O_{40} = 35J_z^4 - [30J(J+1) - 25]J_z^2 + 3J^2(J+1)^2$$
$$- 6J(J+1), \tag{11}$$

$$O_{44} = \tfrac{1}{2}(J_+^4 + J_-^4), \tag{12}$$

suggesting that it is a robust consequence of triplet-doublet splitting, with T_s reflecting single-ion physics; in this model, $|\Delta| = 120|V_{\text{eff}}|$. Varying the doublet-triplet splitting, we find $k_B T_s \approx 0.35|\Delta|$, while the crossover from the high temperature Curie-Weiss-like form to the low temperature behavior occurs at a temperature T_{cr} given by $k_B T_{\text{cr}} \approx 0.07|\Delta|$.

Remarkably, precisely such a behavior, with a Curie-Weiss-like form for $\chi^{-1}(T)$ and a break in slope on going below $\lesssim 150$ K has been observed [31] in Ba_2YReO_6, leading us to suspect that the experimentally reported large Curie-Weiss temperature ~ -600 K may in fact be misleading, and could partly reflect this modified single-ion physics. The true Curie-Weiss temperature in this material may thus well be much smaller, and likely closer to that seen in the d^2 osmates discussed above. Our exploration thus serves to partly rationalize the widely diverging Curie-Weiss temperatures reported in this class of materials as arising from the differences in the single-ion physics of different $5d$ ions. The nature and strength of exchange interactions between such magnetic ions will be discussed elsewhere, in the context of ongoing experiments on Ba_2YReO_6.

IV. DISCUSSION

We have shown that the physics of spin-orbit coupled $J = 2$ magnets can exhibit unconventional multipolar orders which emerge from a low energy non-Kramers doublet. This doublet arises from crystal field splitting of the $J = 2$ multiplet due to multiple physical effects: weak t_{2g}-e_g mixing as well as deviation of the Coulomb interaction from spherical symmetry. Ferro-octupolar ordering within this doublet, which can result from the interplay of magnetic exchange and orbital repulsion [19], provides the most viable explanation for the huge body of experimental data, including the μSR oscillations which we have shown results from orbital electronic currents. As a further test of our theory, we propose that nuclear magnetic resonance (NMR) studies on the oxygen site should show no sign of any internal fields below T^* due to its octupolar structure, which is evident from the schematic plot in Fig. 4; specifically, the octupolar configuration in a cubic system is invariant under C_4 rotations about the Os-O

axis followed by time reversal. This vanishing of the field in oxygen NMR would serve to further distinguish octupolar order from possible dipolar order for which we do expect to see an internal field in the NMR spectrum. Applying uniaxial pressure along the $\langle 111 \rangle$ or $\langle 110 \rangle$ directions would break this C_4 symmetry, leading to a nonzero field at the oxygen site which may be detectable by NMR. In previous work [19] we have also shown how Raman scattering in a $\langle 111 \rangle$ magnetic field can uncover octupolar order via the appearance of new modes below T^*. Our work makes a compelling case for octupolar order in a d-orbital Mott insulator. Future experimental studies using pressure or doping, to suppress the octupolar transition temperature and induce metallicity, may allow one to study possible non-Fermi liquid states associated with fluctuating multipolar orders [37]. Our work emphasizes the need for additional *ab initio* studies of $5d$ oxides at various filling factors to construct the appropriate Wannier functions in order to extract the local interaction Hamiltonian. In light of our work, it is also imperative to revisit the entire body of experiments on other $5d^2$ materials, such as Ba_2YReO_6, as well as $5d$ oxides at other filling factors.

APPENDIX A: ORBITAL WAVE FUNCTIONS AND L MATRICES

The d orbital basis is constructed out of the l_z eigenstates of the angular momentum $l = 2$ manifold as

$$
\begin{aligned}
|yz\rangle &= \frac{i}{\sqrt{2}}(|-1\rangle + |1\rangle) \equiv |1\rangle_\alpha, \\
|xz\rangle &= \frac{1}{\sqrt{2}}(|-1\rangle - |1\rangle) \equiv |2\rangle_\alpha, \\
|xy\rangle &= \frac{i}{\sqrt{2}}(|-2\rangle - |2\rangle) \equiv |3\rangle_\alpha, \\
|x^2 - y^2\rangle &= \frac{1}{\sqrt{2}}(|-2\rangle + |2\rangle) \equiv |4\rangle_\alpha, \\
|3z^2 - r^2\rangle &= |0\rangle \equiv |5\rangle_\alpha,
\end{aligned}
\tag{A1}
$$

where the states $|m\rangle$ refer to $|l = 2, m\rangle$ and states with the subscript α indicate the orbital basis. Since this is the basis we will be working with in this paper, the α index will be dropped. The $|m\rangle$ states in position space can be represented using spherical harmonics (employing the Condon-Shortley phase), and the particular linear combinations above ensure that the orbital wave functions are real, giving the so-called tesseral harmonics. In this basis, the angular momentum

matrices can be constructed as

$$
L_x = \left(\begin{array}{ccc|cc}
0 & 0 & 0 & -i & -i\sqrt{3} \\
0 & 0 & i & 0 & 0 \\
0 & -i & 0 & 0 & 0 \\
\hline
i & 0 & 0 & 0 & 0 \\
i\sqrt{3} & 0 & 0 & 0 & 0
\end{array}\right),
$$

$$
L_y = \left(\begin{array}{ccc|cc}
0 & 0 & -i & 0 & 0 \\
0 & 0 & 0 & -i & i\sqrt{3} \\
i & 0 & 0 & 0 & 0 \\
\hline
0 & i & 0 & 0 & 0 \\
0 & -i\sqrt{3} & 0 & 0 & 0
\end{array}\right), \quad \text{(A2)}
$$

$$
L_z = \left(\begin{array}{ccc|cc}
0 & i & 0 & 0 & 0 \\
-i & 0 & 0 & 0 & 0 \\
0 & 0 & 0 & 2i & 0 \\
\hline
0 & 0 & -2i & 0 & 0 \\
0 & 0 & 0 & 0 & 0
\end{array}\right).
$$

The top left blocks in the above matrices show the t_{2g} subspace, and it is clear that the angular momentum is completely quenched in the e_g subspace.

APPENDIX B: PERTURBATION THEORY

We carry out a perturbation theory study, using H_{CEF} [Eq. (2)] as the unperturbed Hamiltonian and treating J_H (interactions) and λ (SOC) as perturbations. Working in the two-electron basis $|\alpha_1, s_1; \alpha_2, s_2\rangle \equiv c^\dagger_{\alpha_1, s_1} c^\dagger_{\alpha_2, s_2} |0\rangle$, where the α's are orbital indices, and the s's are spin indices, the unperturbed eigenspace consists of three energy levels $\{0, V_C, 2V_C\}$, with degeneracies $\{15, 24, 6\}$. These correspond to double occupancy within the t_{2g} level, shared occupancy between the t_{2g} and e_g levels, and double occupancy in the e_g level, respectively. The perturbations couple these different sectors. For instance, SOC can excite an electron from a t_{2g} level into an e_g level, across the gap V_C. Similarly, pair hopping can hop a pair of electrons from a t_{2g} level into an e_g level, across an energy gap $2V_C$. Treating such terms within perturbation theory we find that in order to project out the e_g subspace, we treat all such mixing terms adding second-order and third-order perturbation effects, which leads to an effective t_{2g} subspace Hamiltonian. At second order, we find that $U' - U$, pair hopping, and magnetic Hund's coupling are renormalized differently, but in a way that does not break spherical symmetry, i.e., the renormalized Kanamori couplings obey [32] $U' - U = J_P + J_H$ (where J_P and J_H denote, respectively, the strength of the interorbital pair hopping and magnetic Hund's coupling). Diagonalizing the resulting effective Hamiltonian, which sums the full Hamiltonian projected to t_{2g} levels with the above perturbed interactions, we find that the ground state remains a fivefold degenerate $J = 2$ multiplet. However, at third order, we find new interactions that arise in the effective Hamiltonian in the t_{2g} manifold which cannot be described as renormalizations of existing interactions; specifically, there

are terms schematically given by

$$
\Delta H^{(3)}_{L,L'} = \sum_{H,H'} \frac{(H_{\text{SOC}})_{L,H}(H_{\text{Hund}})_{H,H'}(H_{\text{SOC}})_{H',L'}}{V_C^2},
$$

where L, H refer to low and high energy states with L having both electrons in the t_{2g} orbitals, and H having one electron in t_{2g} and the other in e_g. This term leads to a splitting of the $J = 2$ manifold into a low energy non-Kramers doublet and a high energy magnetic triplet, with the splitting emerging at $O(\lambda^2 J_H / V_C^2)$ at large V_C.

APPENDIX C: ORBITAL CURRENTS AND MAGNETIC FIELDS

In order to study the impact of ferro-octupolar order in generating time-reversal breaking electronic currents and magnetic fields, we explicitly write out the orbital wave functions in position space which enter the angular momentum states. For this, we multiply the radial part of the hydrogenlike wave function with the tesseral harmonic of the orbital. We use the following form for the radial wave function:

$$
R_{nl}(r) = N_{nl} \, \rho^l(r) e^{-\rho(r)/2} L^{2l+1}_{n-l-1}[\rho(r)], \quad \text{(C1)}
$$

where n is the principal quantum number, l is the angular momentum quantum number, and $\rho(r) = 2r/na(r)$. L^{2l+1}_{n-l-1} is the generalized Laguerre polynomial, and N_{nl} is a normalization constant. $a(r)$ is a function which captures the screening by the inner electrons, which we call the "effective" Bohr radius. The function must be chosen such that

$$
\lim_{r \to 0} a(r) = a_0/Z_0; \quad \lim_{r \to \infty} a(r) = a_0/Z_\infty, \quad \text{(C2)}
$$

where a_0 is the (hydrogen) Bohr radius, Z_0 is the bare charge of the nucleus, and Z_∞ is the effective charge that an electron sees at large distances. We propose the following simple form:

$$
a(r) = \frac{a_0}{Z(r)}; \quad Z(r) = Z_\infty + (Z_0 - Z_\infty)e^{-r/r_0}, \quad \text{(C3)}
$$

with r_0 being a tuning parameter which determines how the effective charge falls off with distance. For instance, for an Os^{6+} ion, $Z_0 = 76$ and $Z_\infty = 7$ (since all electrons except the one $5d$ electron we focus on will contribute to screening at large distances). A reasonable value for r_0 is that it is smaller than the ionic radius ~ 70 pm; we thus consider $r_0 = 10$–20 pm. If we are interested in $5d$ electrons, the radial wave function is of the form

$$
R_{52}(r) = N_{52} \left(\frac{2r}{5a(r)}\right)^2 e^{-r/5a(r)} L^5_2\left(\frac{2r}{5a(r)}\right). \quad \text{(C4)}
$$

The normalization constant N_{52} depends on r_0. Hence the full wave function is given by $\psi_{nl\alpha} = R_{nl}(r) Y_{l\alpha}(\theta, \phi)$, where $Y_{l\alpha}$ is the tesseral harmonic associated with the α orbital. The current operator thus becomes

$$
\mathbf{J} = \frac{ie\hbar}{2m} \sum_{\alpha,\beta} \sum_s (\psi_{nl\alpha} \nabla \psi_{nl\beta} - \psi_{nl\beta} \nabla \psi_{nl\alpha}) c^\dagger_{\alpha,s} c_{\beta,s}. \quad \text{(C5)}
$$

All the spatial dependence of the current is encoded in the factor $\psi_{nl\alpha} \nabla \psi_{nl\beta} - \psi_{nl\beta} \nabla \psi_{nl\alpha} \equiv \boldsymbol{\xi}_{\alpha\beta}(r, \theta, \phi)$. Since the wave functions can be separated into the radial and angular

components, i.e., $\psi_{nl\alpha} = R_{nl}(r)Y_{l\alpha}(\theta, \phi)$, this factor becomes

$$\boldsymbol{\xi}_{\alpha\beta} = R_{nl}^2(Y_{l\alpha}\nabla Y_{l\beta} - Y_{l\beta}\nabla Y_{l\alpha}). \tag{C6}$$

From the exact diagonalization, we can obtain the ground state of the system as some linear combination of our basis states. Let us call this ground state $|\psi_g\rangle$:

$$|\psi_g\rangle = \sum_{\Omega} a_{\Omega} |\Omega\rangle, \tag{C7}$$

where $|\Omega\rangle$ refers to our basis states of the form $|\alpha_1, s_1; \alpha_2, s_2\rangle$. Since we are interested in the matrix elements of the current

in Eq. (C5) in this state, we can recast the problem as

$$\langle \mathbf{J} \rangle = \frac{ie\hbar}{2m} \sum_{\alpha,\beta} w_{\alpha\beta}\, \boldsymbol{\xi}_{\alpha\beta}, \tag{C8}$$

where each factor $\boldsymbol{\xi}_{\alpha\beta}$ is associated with a "weight" $w_{\alpha\beta}$, given by

$$w_{\alpha\beta} = \sum_{\Omega,\Omega'} a_{\Omega}^* a_{\Omega'} \sum_s \langle \Omega | c_{\alpha,s}^\dagger c_{\beta,s} | \Omega' \rangle. \tag{C9}$$

It can be seen that $w_{\alpha\beta} = w_{\beta\alpha}^*$. The Hermiticity of $\mathbf{J}$ constrains the weights to be purely imaginary. Once the expectation value of the current density is obtained, we use Eq. (10) to compute the magnetic field.

[1] P. Santini, S. Carretta, G. Amoretti, R. Caciuffo, N. Magnani, and G. H. Lander, Rev. Mod. Phys. **81**, 807 (2009).

[2] K. Haule and G. Kotliar, Nat. Phys. **5**, 796 (2009).

[3] P. Santini and G. Amoretti, Phys. Rev. Lett. **85**, 2188 (2000).

[4] J. A. Paixão, C. Detlefs, M. J. Longfield, R. Caciuffo, P. Santini, N. Bernhoeft, J. Rebizant, and G. H. Lander, Phys. Rev. Lett. **89**, 187202 (2002).

[5] A. Kiss and P. Fazekas, Phys. Rev. B **68**, 174425 (2003).

[6] Y. Tokunaga, D. Aoki, Y. Homma, S. Kambe, H. Sakai, S. Ikeda, T. Fujimoto, R. E. Walstedt, H. Yasuoka, E. Yamamoto, A. Nakamura, and Y. Shiokawa, Phys. Rev. Lett. **97**, 257601 (2006).

[7] T.-h. Arima, J. Phys. Soc. Jpn. **82**, 013705 (2013).

[8] A. Sakai and S. Nakatsuji, J. Phys. Soc. Jpn. **80**, 063701 (2011).

[9] T. J. Sato, S. Ibuka, Y. Nambu, T. Yamazaki, T. Hong, A. Sakai, and S. Nakatsuji, Phys. Rev. B **86**, 184419 (2012).

[10] M. Tsujimoto, Y. Matsumoto, T. Tomita, A. Sakai, and S. Nakatsuji, Phys. Rev. Lett. **113**, 267001 (2014).

[11] K. Hattori and H. Tsunetsugu, J. Phys. Soc. Jpn. **85**, 094001 (2016).

[12] F. Freyer, J. Attig, S. Lee, A. Paramekanti, S. Trebst, and Y. B. Kim, Phys. Rev. B **97**, 115111 (2018).

[13] S. Lee, S. Trebst, Y. B. Kim, and A. Paramekanti, Phys. Rev. B **98**, 134447 (2018).

[14] A. S. Patri, A. Sakai, S. Lee, A. Paramekanti, S. Nakatsuji, and Y. B. Kim, Nat. Commun. **10**, 4092 (2019).

[15] L. Fu, Phys. Rev. Lett. **115**, 026401 (2015).

[16] J. W. Harter, Z. Y. Zhao, J.-Q. Yan, D. G. Mandrus, and D. Hsieh, Science **356**, 295 (2017).

[17] S. Hayami, H. Kusunose, and Y. Motome, Phys. Rev. B **97**, 024414 (2018).

[18] D. D. Maharaj, G. Sala, M. B. Stone, E. Kermarrec, C. Ritter, F. Fauth, C. A. Marjerrison, J. E. Greedan, A. Paramekanti, and B. D. Gaulin, Phys. Rev. Lett. **124**, 087206 (2020).

[19] A. Paramekanti, D. D. Maharaj, and B. D. Gaulin, Phys. Rev. B **101**, 054439 (2020).

[20] G. Chen, R. Pereira, and L. Balents, Phys. Rev. B **82**, 174440 (2010).

[21] G. Chen and L. Balents, Phys. Rev. B **84**, 094420 (2011).

[22] C. Svoboda, M. Randeria, and N. Trivedi, Phys. Rev. B **95**, 014409 (2017).

[23] C. M. Thompson, J. P. Carlo, R. Flacau, T. Aharen, I. A. Leahy, J. R. Pollichemi, T. J. S. Munsie, T. Medina, G. M. Luke, J. Munevar, S. Cheung, T. Goko, Y. J. Uemura, and J. E. Greedan, J. Phys.: Condens. Matter **26**, 306003 (2014).

[24] E. Kermarrec, C. A. Marjerrison, C. M. Thompson, D. D. Maharaj, K. Levin, S. Kroeker, G. E. Granroth, R. Flacau, Z. Yamani, J. E. Greedan, and B. D. Gaulin, Phys. Rev. B **91**, 075133 (2015).

[25] C. M. Thompson, C. A. Marjerrison, A. Z. Sharma, C. R. Wiebe, D. D. Maharaj, G. Sala, R. Flacau, A. M. Hallas, Y. Cai, B. D. Gaulin, G. M. Luke, and J. E. Greedan, Phys. Rev. B **93**, 014431 (2016).

[26] C. A. Marjerrison, C. M. Thompson, A. Z. Sharma, A. M. Hallas, M. N. Wilson, T. J. S. Munsie, R. Flacau, C. R. Wiebe, B. D. Gaulin, G. M. Luke, and J. E. Greedan, Phys. Rev. B **94**, 134429 (2016).

[27] G. L. Stamokostas and G. A. Fiete, Phys. Rev. B **97**, 085150 (2018).

[28] T. Ribic, E. Assmann, A. Tóth, and K. Held, Phys. Rev. B **90**, 165105 (2014).

[29] B. Yuan, J. P. Clancy, A. M. Cook, C. M. Thompson, J. Greedan, G. Cao, B. C. Jeon, T. W. Noh, M. H. Upton, D. Casa, T. Gog, A. Paramekanti, and Y.-J. Kim, Phys. Rev. B **95**, 235114 (2017).

[30] A. Paramekanti, D. J. Singh, B. Yuan, D. Casa, A. Said, Y.-J. Kim, and A. D. Christianson, Phys. Rev. B **97**, 235119 (2018).

[31] T. Aharen, J. E. Greedan, C. A. Bridges, A. A. Aczel, J. Rodriguez, G. MacDougall, G. M. Luke, V. K. Michaelis, S. Kroeker, C. R. Wiebe, H. Zhou, and L. M. D. Cranswick, Phys. Rev. B **81**, 064436 (2010).

[32] A. Georges, L. d. Medici, and J. Mravlje, Annu. Rev. Condens. Matter Phys. **4**, 137 (2013).

[33] M. E. Simon and C. M. Varma, Phys. Rev. Lett. **89**, 247003 (2002).

[34] P. Chandra, P. Coleman, J. A. Mydosh, and V. Tripathi, Nature (London) **417**, 831 (2002).

[35] W. K. Dawson, K. Tibbs, S. P. Weathersby, C. Boekema, and K. B. Chan, J. Appl. Phys. **64**, 5809 (1988).

[36] F. R. Foronda, F. Lang, J. S. Möller, T. Lancaster, A. T. Boothroyd, F. L. Pratt, S. R. Giblin, D. Prabhakaran, and S. J. Blundell, Phys. Rev. Lett. **114**, 017602 (2015).

[37] A. S. Patri, I. Khait, and Y. B. Kim, Phys. Rev. Res. **2**, 013257 (2020).

Correction: The previously published Fig. 6 contained y-axis scale errors and was replaced.